WATER RESOURCES RESEARCH, VOL. 33, NO. 4, PAGES 711–724, APRIL 1997

Streamflow simulation for continental-scale river basins

Bart Nijssen and Dennis P. Lettenmaier
Department of Civil Engineering, University of Washington, Seattle

Xu Liang, Suzanne W. Wetzel,[1] and Eric F. Wood
Department of Civil Engineering and Operations Research, Princeton University, Princeton, New Jersey

Abstract. A grid network version of the two-layer variable infiltration capacity (VIC-2L) macroscale hydrologic model is described. VIC-2L is a hydrologically based soil-vegetation-atmosphere transfer scheme designed to represent the land surface in numerical weather prediction and climate models. The grid network scheme allows streamflow to be predicted for large continental rivers. Off-line (observed and estimated surface meteorological and radiative forcings) applications of the model to the Columbia River (1° latitude-longitude spatial resolution) and Delaware River (0.5° resolution) are described. The model performed quite well in both applications, reproducing the seasonal hydrograph and annual flow volumes to within a few percent. Difficulties in reproducing observed streamflow in the arid portion of the Snake River basin are attributed to groundwater-surface water interactions, which are not modeled by VIC-2L.

1. Introduction

The evolution of continental-scale hydrology has placed a new set of demands on hydrologic modelers. Atmospheric general circulation models (GCMs) used for climate simulation and numerical weather prediction require explicit representation of processes occurring at the land surface. The role of soil moisture and vegetation in partitioning net radiation into sensible and latent heat, and precipitation into evapotranspiration and runoff, is especially important. As noted by *Wood* [1991], this requirement has led to the development of land surface schemes for GCMs that emphasize vertical complexity and largely neglect horizontal heterogeneities, notwithstanding the extreme variability in land surface characteristics that occurs within the GCM spatial scale, which is typically on the order of 100 km or more.

Over the last 10 years there has been an explosion of research activity aimed at improving GCM land surface schemes. Over 30 such schemes are presently participating in the Project for Intercomparison of Land Surface Parameterization Schemes (PILPS) [*Henderson-Sellers et al.*, 1995]. However, much of the attention in these efforts has been focused on the ability of the schemes to partition surface energy correctly over a range of climates, land surface characteristics, and soil moisture stress. While this emphasis is consistent with the role the land surface plays in affecting atmospheric circulation, it largely ignores important diagnostic and water management implications of GCM land surface schemes.

In this paper we focus instead on the ability of the two-layer variable infiltration capacity macroscale hydrologic model (VIC-2L) [*Liang et al.*, 1994] to predict streamflow for continental river basins, which we somewhat arbitrarily define as those basins having drainage areas in the range 25,000–1,000,000 km^2. Prediction of streamflow at such scales is of interest for at least three reasons. First, streamflow is a spatial integrator of hydrological processes and as such offers the opportunity to verify the GCM surface water balance. Streamflow is arguably the easiest component of the surface water balance to measure directly. It is routinely measured at a number of points on the world's major rivers, and these observations could provide a basis for evaluating the performance of GCMs on a climatological basis and of weather prediction models in near real time. In this work we limit ourselves to off-line simulations; that is, we drive our model with observed meteorological data (precipitation and temperature) and estimated radiative forcings, in contrast to on-line simulation, in which the land surface scheme is incorporated directly in a GCM. Our motivation is to demonstrate that the model can produce accurate streamflow simulations with observational data; thus model results produced from on-line simulations should provide a useful diagnostic for GCM surface water balances, as any errors will be attributable primarily to errors in GCM surface forcings. In this respect the work reported here can be considered a precursor to on-line diagnostic studies of the water balance inferred from numerical weather prediction models for large continental rivers.

A second reason for interest in the simulation of large continental rivers is their effect on the surface salinity of the polar oceans and, consequently, sea ice formation. The freshwater flux from land to ocean has important implications for the thermohaline circulation [*Sausen et al.*, 1994; *Dümenil and Todeni*, 1992]. Off-line simulations, such as those described in this paper, should be directly relevant to projects such as the Arctic Climate System Study [*World Meteorological Organization (WMO)*, 1994], which seeks to improve estimates of the freshwater inflows to the Arctic Ocean.

A third reason for interest in simulation of large continental rivers is that this capability has water management implications in its own right. Operational forecasting tools already exist, and are routinely applied to large rivers. For instance, the U.S. National Weather Service uses the National Weather Service River Forecast System (NWSRFS) to forecast streamflows at a

[1]Now at Applied Ocean Physics and Engineering Department, Woods Hole Oceanographic Institution, Woods Hole, Massachusetts.

Paper number 96WR03517.
0043-1397/97/96WR-03517.

number of points in large rivers such as the Columbia and Arkansas-Red. Their approach typically is to link together applications of a conceptual streamflow simulation model, for example, the Sacramento Model [*Burnash et al.*, 1973], for subbasins in such a way as to produce forecasts at selected control points. The difficulty with this approach is that it tends to be piecemeal and labor intensive. For instance, applying NWSRFS to the Columbia basin [*Riverside Technologies, Inc.*, 1994] required calibration of the model for over 100 subbasins. More importantly, conceptual streamflow simulation models are inherently incompatible with GCMs. We anticipate that as numerical weather prediction models, and especially the capabilities of long-term weather forecasts, evolve, there will be a requirement for consistent streamflow forecasts for water management applications. Macroscale hydrologic models that also are capable of serving as land surface schemes will be needed to serve this need.

Several recent papers describe the use of simple river routing schemes to predict the long-term mean runoff from major world rivers [*Russel and Miller*, 1990; *Kuhl and Miller*, 1992; *Miller et al.*, 1994; *Dümenil and Todeni*, 1992; *Sausen et al.*, 1994; *Liston et al.*, 1994]. Where GCM runoff is used as the input to the routing schemes, large errors typically result in the predictions. The sources of the errors are difficult to identify, as either errors in the inputs (precipitation) or in the land surface scheme may be to blame. The off-line scheme we use in this paper helps define the magnitude of the simulation errors that can be expected, when the forcings are as well known as is possible given the limitations of the observational data. Applications to two North American river basins are presented. The first is the Columbia River, in the Pacific Northwest (drainage area 669,000 km^2), which is dominated by winter snow accumulation and spring melt. The second is the much smaller Delaware River, in the eastern United States (drainage area 33,100 km^2), which has a more even distribution of precipitation throughout the year and where snow plays a more limited role.

2. Modeling Approach and Model Description

The VIC-2L model was developed as a soil-vegetation-atmosphere transfer scheme (SVATS) for GCMs [*Liang et al.*, 1994]. As compared with other SVATS, its distinguishing features are that it represents the subgrid variability in soil moisture storage capacity as a spatial probability distribution, and drainage from a lower soil moisture zone (base flow) as a nonlinear recession. VIC-2L is a generalization of a single soil-layer model, variations of which have previously been employed in the Max Planck Institute [*Dümenil and Todeni*, 1992], the Geophysical Fluid Dynamics Laboratory [*Stamm et al.*, 1994], and the UK Meteorological Office [*Rowntree and Lean*, 1994] GCMs. When the VIC-2L model is run on-line in a GCM (using its energy balance mode), it predicts both land surface water and energy fluxes, and is driven by incoming radiation, precipitation, air temperature, humidity, and wind. In off-line applications, such as those described here, the model is driven by precipitation, and maximum and minimum temperature at a daily time step and predicts evaporation, surface, and subsurface runoff (water balance mode). Net shortwave and longwave radiation are parameterized in terms of daily minimum and maximum temperature, but the energy balance snow model of *Wigmosta et al.* [1994], which is used in on-line applications, is replaced with the temperature index NWSRFS snow accumulation and ablation model [*Anderson*, 1973]. The snow model simulates the snowpack dynamics, resulting in a rain-plus-melt series which serves as the effective precipitation input for the VIC-2L model.

The first step in application of the river network water balance version of VIC-2L is to divide the river basin into grid cells (1° × 1° latitude by longitude in the case of the Columbia and 0.5° × 0.5° in the case of the Delaware). Using the output from the snow model, VIC-2L is applied to simulate the total daily runoff and evapotranspiration for each grid cell independently. The runoff from each of the individual cells is then combined using a routing scheme, based on simple distance and travel time assumptions, to produce daily and then accumulated monthly flows at selected calibration points. The three elements of this modeling approach (snow, land surface hydrology, and routing models) are described in more detail below.

2.1. Temperature Index Snow Accumulation and Ablation Model

The NWSRFS temperature index model uses mean areal air temperature as the sole index to the energy exchange at the snow-air interface [*Anderson*, 1973]. Surface air temperature and precipitation are the only meteorological inputs required. However, in contrast to other temperature index approaches based on the degree-day method [*Gray and Prowse*, 1993], all significant physical processes, such as heat exchange at the snow-air interface, snowpack heat storage, and melt during rain on snow events, are represented explicitly. Snowmelt during nonrain periods is assumed to be linearly related to the difference between the air temperature and a base temperature, normally 0°C, according to a seasonally varying melt factor, which has a minimum in December and a maximum in June. During rain-on-snow events the amount of melt is calculated using an energy balance approach. The areal extent of the snow cover is modeled using snow cover depletion curves, which relate the amount of snow-covered area to the average snow water equivalent. Snow sublimation and snow interception by the vegetation are not represented.

In mountainous areas, total snow water equivalent and snow cover extent vary strongly with elevation as a result of temperature changes and orographic precipitation effects. To capture some of the snow accumulation and ablation dynamics in mountainous areas, each grid cell was subdivided into four elevation bands of equal area. The air temperature was lapsed from the mean grid cell elevation to the median elevation of each band using a lapse rate of 6°C/km, and the precipitation was allowed to vary with elevation as well. A 6-hour computational time step was used to represent the diurnal cycle because of the importance of capturing melt during the day and refreezing during the night and diurnal differences in rain-snow partitioning. Six hourly precipitation values were taken to be one quarter of the daily precipitation, that is, constant precipitation rate during days with precipitation. Six hourly temperature values were calculated from daily minimum and maximum temperatures by imposing a diurnal cycle. The melt series output from the snow model was then aggregated to a daily time step to serve as effective daily precipitation for the VIC-2L model.

2.2. Grid-Based VIC-2L Model

The VIC-2L model is distinguished from other SVATS such as BATS (biosphere-atmosphere transfer scheme) [*Dickinson et al.*, 1986] and SiB (simple biosphere model) [*Sellers et al.*,

1986] in that it uses a spatially varying infiltration capacity based on the Xinanjiang model [*Zhao et al.*, 1980] to represent subgrid-scale heterogeneity in soil properties and hence in moisture storage, evaporation, and runoff production [*Liang et al.*, 1994]. By using a probability distribution of the beta distributional form, the model represents spatial heterogeneity at scales smaller than the application scale, without assigning specific infiltration capacity values to specific subgrid-scale locations. Instead the shape of the spatial probability distribution function is determined by a single parameter, which characterizes the amount of available infiltration capacity as a function of relative saturated grid cell area. Precipitation in excess of the infiltration capacity becomes surface runoff.

Because vegetation exerts important controls on the exchange of water and energy at the land surface, it needs to be explicitly incorporated in land surface parameterization schemes. Each grid cell can have partial surface coverage by a number of different vegetation types, as well as bare soil. Vegetation characteristics, such as leaf area index (LAI), minimum stomatal resistance, roughness length, and displacement length are assigned for each vegetation type, if desirable as a function of time, as in the case of LAI. Evapotranspiration is calculated according to a combination equation approach (Penman-Monteith equation); that is, evapotranspiration is calculated as a function of net radiation and vapor pressure deficit. Following *Brutsaert* [1982], no atmospheric stability correction is applied when using this approach at the daily timescale. In water balance mode, net radiation and vapor pressure deficit are not directly available, and are parameterized as a function of the daily maximum and minimum temperature. Potential radiation at the top of the atmosphere is calculated as a function of latitude, and Julian day [*Shuttleworth*, 1993]. The potential radiation is attenuated through the atmosphere on the basis of atmospheric transmissivity, τ, which is estimated as a function of the diurnal temperature range [*Bristow and Campbell*, 1984] according to

$$\tau = A[1 - \exp(B\Delta T^C)]$$

where ΔT is the diurnal temperature range in degrees Celsius, A is the maximum clear sky transmittance, and B and C are empirical constants. Values for A, B, and C were based on work by *Bristow and Campbell* [1984]. In the absence of information about the atmospheric humidity profile, the daily minimum temperature was used to approximate the dew point temperature. The vapor pressure deficit can then be calculated as

$$D = e_s(T_{\text{air}}) - e_s(T_{\text{min}})$$

where D is the vapor pressure deficit in pascals, e_s is the saturated vapor pressure in pascals, T_{air} is the average daily air temperature in degrees Celsius, and T_{min} is the daily minimum air temperature in degrees Celsius. Although this approximation is reasonably accurate in humid climates [*Kimball et al.*, 1997], it does not hold in more arid climates, where nighttime minimum temperatures often remain above the dew point temperature. Thus a correction was applied to $e_s(T_{\text{min}})$ in semiarid and arid areas according to *Kimball et al.* [1997]. Their approach uses the ratio of yearly Priestley-Taylor potential evaporation (which only depends on net radiation) to yearly precipitation as an aridity index. For locations where this index is less than 2.25, no correction to $e_s(T_{\text{min}})$ is suggested, while for other locations a correction is made on the basis of the ratio of daily Priestley-Taylor potential evaporation to mean daily precipitation and the mean daily air temperature. This correction reduces vapor pressure estimation errors by up to 80%. Net longwave radiation is estimated according to *Bras* [1990], using T_{air} as an approximation for surface temperature, and the previously calculated atmospheric transmissivity, τ, as a measure of cloudiness.

Total actual evapotranspiration is calculated as the sum of canopy evaporation, transpiration from each vegetation class, and bare soil evaporation, weighted by the fraction of surface area for each surface cover class. In concept, this approach is similar to what has been termed alternatively "the mosaic approach" in the land surface modeling community [e.g., *Koster and Suarez*, 1992], and "the grouped response unit method" by the hydrologic modeling community [e.g., *Kouwen et al.*, 1993].

Precipitation intercepted by the canopy is allowed to evaporate at the potential rate, adjusted for canopy and architectural resistances in the manner described by *Ducoudré et al.* [1993]. Transpiration is estimated using the formulation of *Blondin* [1991] and *Ducoudré et al.* [1993], which incorporates canopy resistance (including soil moisture, temperature, and vapor pressure deficit limitations), aerodynamic resistance, and architectural resistances. The architectural resistance represents the aerodynamic resistance between the leaves and the canopy top, to account for an imperfectly ventilated canopy [*Ducoudré et al.*, 1993]. Bare soil evaporation is modeled using the Arno formulation [*Francini and Pacciani*, 1991]. Canopy interception follows a BATS parameterization [*Dickinson et al.*, 1986], in which the amount of canopy interception is a function of LAI. The subsurface scheme consists of two soil layers. The upper layer receives moisture from precipitation through infiltration. Transport from the first soil layer to the second occurs through gravity drainage, regulated by a Brooks-Corey relationship for the unsaturated hydraulic conductivity. The second soil layer receives moisture from the upper layer and contributes to runoff using a drainage formulation based on the Arno model [*Francini and Pacciani*, 1991]. Moisture can also be extracted from either or both soil layers by evapotranspiration, depending on the prescribed fraction of roots in each zone. For each grid cell VIC-2L is run at a daily time step, using the rain-plus-melt output time series from the snow model (averaged over the four elevation bands) as its precipitation input.

To assess whether a daily time step could be used for the calculation of potential evapotranspiration using the Penman-Monteith equation, potential evaporation was calculated for two surface airways stations in the northwestern United States on both hourly and daily timescales. The hourly values were then aggregated to the daily timescale to compare with the daily values calculated on the basis of average daily meteorological conditions. The potential evaporation values calculated at the daily timescale were on average 5.7% (0.13 mm/day) lower than those calculated on the hourly timescale for SeaTac Airport in western Washington State. For Boise, Idaho, which is characterized by a drier and more continental climate, the values calculated at a daily time step were 7.4% (0.26 mm/day) lower than those calculated at an hourly time step. Although this difference is not negligible, the fractional changes are expected to be smaller for actual evaporation than for potential, which does not account for soil moisture stress and vegetation effects. In addition, much of the evaporation in the Columbia River basin is moisture limited, and the error intro-

duced by using the Penman-Monteith equation at the daily time step is well within the accuracy of the other parameterizations used in the model.

2.3. Routing Model

Although the grid-based version of VIC-2L produces only one time series of runoff values for each grid cell, this runoff should not be considered as being produced at a single point, but as being distributed nonuniformly over the area of that grid cell, in accordance with the antecedent distribution of soil moisture and soil moisture capacity. To account for differences in travel time of runoff produced in different parts of the grid cell, the daily runoff produced by VIC-2L is convolved with a triangular unit hydrograph, which simulates routing within the grid cell. The hydrographs produced for each grid cell are then routed to the basin outlet. The channel network linking the individual grid cells is schematized at the 1° or 0.5° grid scale by connecting the centers of the grid cells following the main direction of flow, as determined from maps. For cells on the edge of the basin the relative area of the grid cell lying inside the basin can be specified, allowing the modeled area to be equal to the basin area. Each cell can flow into any one of its eight neighbors, but all flow has to exit in the same direction. The outflow from each cell is added to the downstream cell, with a time delay based on a simple travel distance and velocity assumption, after convolving the outflow with a unit impulse response function. In our schematic representation of the river network the travel distance is taken as the shortest distance between the centers of the grid cells between which transport is taking place. A linear reservoir model with a small reservoir coefficient was selected for the impulse response function.

Because the discharge pattern of many large rivers is regulated by storage in man-made reservoirs, the routing model also allows for the explicit representation of such reservoirs. Total reservoir capacity and minimum release rates can be specified for each grid cell, and the flow is routed through the reservoir before entering the downstream grid cell [*Wetzel*, 1994]. In the applications discussed in this paper, naturalized river flows were used. These naturalized flows are based on observed river flows but are corrected for reservoir storage effects, reservoir evaporation, and withdrawals for irrigation. Thus the natural flows represent what the observed flow would have been if reservoirs had not been present in the basin and if no withdrawals and/or diversions had occurred. Reservoir routing is therefore not needed, and the reservoir storage capacities were all set to zero.

3. Basin Descriptions

3.1. Columbia River Basin

The Columbia River drains an area of 567,000 km^2 of seven states in the western United States (Washington, Oregon, Idaho, Montana, Wyoming, Nevada, and Utah) as well as 102,000 km^2 of British Columbia, in western Canada. The climate ranges from moist, maritime conditions in the western parts of the basin to semiarid and arid conditions in the southeastern part. Mean annual precipitation varies from more than 2500 mm near the mouth of the river to less than 250 mm in the driest areas, with most of the basin receiving less than 800 mm. Precipitation in the basin is winter dominant, much of which is stored as snow. Consequently, most of the runoff is generated in spring by snowmelt from the mountains surrounding the basin, with peak flows occurring in late May and early June. The water resources in the basin are highly developed, with 162 reservoirs with capacities greater than 6×10^6 m^3 on the main stem and tributaries [*U.S. Geological Survey* (*USGS*), 1994]. The major reservoirs serve multiple functions, including hydropower, irrigation, flood control, and recreation.

3.2. Delaware River Basin

The Delaware River drains an area of 33,100 km^2 of New York, Pennsylvania, New Jersey, and Delaware and is a major source of drinking water for more than 15 million people living in the Atlantic seaboard area of those states. Below Trenton, New Jersey, the Delaware River forms a tidal estuary, which enters the Atlantic Ocean at the mouth of Delaware Bay. The climate of the basin is humid-temperate, with a mean annual temperature of 12°C and a mean annual precipitation of 1200 mm. The mean annual temperature varies from about 7°C in the north to about 13°C in the south, whereas the variation in mean annual precipitation, from 1000 to 1300 mm, is more strongly dependent on elevation than on latitude. Only the northern part of the basin experiences significant snow accumulation [*Ayers et al.*, 1994]. As in the case of the Columbia River, the water resources of the Delaware basin are highly developed. The major reservoirs in the basin are operated to provide municipal water supply, subject to target flows in the Delaware River at Montague and Trenton, which are necessary to prevent saltwater intrusion in the lower part of the basin.

4. Model Implementation

4.1. Topography

Subdivision of each grid cell into four equal-area elevation bands was based on a 30-arcsecond digital elevation model (DEM). Median elevations were determined for each grid cell and for each elevation band. These elevations were used in the snow model to lapse temperature and precipitation from the station elevation to the different elevation bands.

4.2. Meteorological Data

Since the model was employed in water balance mode, the only required meteorological inputs were daily minimum and maximum air temperature, daily precipitation, and wind speed. Because wind observations are available at only a limited number of locations, the use of observed wind speed values is problematic. Instead, average monthly 10-m wind fields from the NCEP/NCAR (National Centers for Environmental Prediction/National Center for Atmospheric Research) Reanalysis Project [*Kalnay et al.*, 1996] were used. These wind fields have a spatial resolution of 2.5° latitude × 2.5° longitude and were interpolated to the appropriate grid cell resolution by interpolating the u and v components of the field separately and then calculating the magnitude. The wind at an elevation of 2 m above the top of the canopy was then calculated assuming a logarithmic velocity profile. The primary data source for daily minimum and maximum air temperature and daily precipitation was work by *Wallis et al.* [1991]. Since this data set, which has been corrected for missing data, contained on average fewer than the target of two stations per grid cell, these stations were supplemented by other stations with a sufficient length of record from *Earthinfo Inc.* [1991].

For the Canadian part of the Columbia basin, data from Atmospheric Environment Canada were used. Ultimately, at least one station was found for each grid cell in the Canadian

Table 1. Vegetation Parameters for the Five Vegetation Classes Present in the Columbia and Delaware River Basins

Vegetation Parameter	Vegetation Type*						
	1	2	3	4	5	6	7
Height h, m	1.0	1.0	1.0	17.0	17.0	20.0	0.5
Coverage, %	100	100	100	100	100	100	10
Roughness length z_0, m	0.1	0.1	0.1	1.7	1.7	2.0	0.05
Displacement height d_0, m	0.63	0.63	0.63	10.71	10.71	12.6	0.315
Fraction of roots in layer 1 f_1, %	90	80	70	50	50	50	80
Fraction of roots in layer 2 f_2, %	10	20	30	50	50	50	20
Minimum leaf resistance r_s, s m^{-1}	110	110	110	120	120	100	80
Architectural resistance r_{arc}, s m^{-1}	3	2	3	40	50	50	2.5

*Vegetation types: 1, cultivated; 2, grass with less than 10% woody cover; 3, grass with 10%–40% woody cover; 4, high-latitude deciduous trees; 5, needleleaf evergreen trees; 6, mixed trees; 7, moss and lichens/shrubs and bare soil.

portion of the basin for the period October 1948 to September 1988, and two for most of the U.S. grid cells, although coverage and length of record were marginal for some of the stations in the northern part of the Columbia basin. The station temperatures were lapsed to the mean elevation of the corresponding grid cell using a lapse rate of 6.0°C/km. For grid cells with two stations the adjusted temperatures were then averaged. Because of the high degree of spatial variability of precipitation fields, station observations cannot be expected to provide reliable estimates of areally averaged precipitation. This is particularly true in mountainous regions where orographic uplifting generally results in an increase in precipitation with elevation and where rain shadow effects result in decreased precipitation amounts on the leeward side of mountain chains. Therefore the station series were used to construct a scaled time series of precipitation events with an annual average equal to 1, and this series was then rescaled by the areally averaged precipitation P_{areal} for each grid cell. For those grid cells with two stations, the normalized series were averaged before rescaling. If the model is implemented at a fairly high resolution in an area with relatively homogeneous precipitation, P_{areal} can be calculated as the average of the mean annual precipitation of the stations in the grid cell. This was the approach followed for the Delaware basin.

In the Columbia basin a different approach was required to estimate P_{areal}, because much of the basin is mountainous and because the model was applied at a 1° × 1° resolution. *Daly et al.* [1994] developed a scheme with the explicit purpose of providing better estimates of areally averaged precipitation in topographically complex terrain: PRISM (precipitation-elevation regressions on independent slopes model). PRISM accounts for the effects of elevation and the spatial scale and patterns of orographic effects by combining station observations with DEM data. Each region is subdivided into smaller areas, or "topographic facets," on the basis of slope orientation. For each of these facets a local precipitation-elevation regression relationship is developed. These regression relationships are then used to estimate the precipitation at the DEM elevations for which no observations are available. PRISM estimates of mean monthly precipitation for the Columbia basin at a 2.5-min resolution [*Daly et al.*, 1994] were summed to calculate the average precipitation for the four elevation bands for each grid cell in the Columbia basin.

4.3. Model Parameters

4.3.1. Snow Model Parameters. For a detailed description of the parameters of the snow model, the reader is referred to *Anderson* [1973]. Most of the parameters were kept constant at the values suggested by Anderson. A temperature lapse rate of 6.0°C/km was used to calculate the air temperature for each elevation band. The amount of precipitation in each elevation band was based on the PRISM estimates for the Columbia. In the case of the Delaware, all elevation bands were assumed to have the same precipitation as the grid cell average.

The gage catch deficiency factor, which accounts for catch deficiencies during snowfall, was set to 1.2 for the Delaware basin in order to compensate for the underestimation of precipitation occurring as snow by unshielded gages. In the Columbia basin the catch deficiency factor was not used, because the gage precipitation was rescaled to the PRISM spatial means. The factors that most directly influenced the rain-plus-melt series produced by the snow model were the minimum and maximum melt factors. These factors determine the minimum and maximum amount of snowmelt that can occur during a time period, with the minimum melt occurring on December 21 and the maximum on June 21. Other conditions being equal, the melt factor tends to be higher for open areas than for forested areas [*Anderson*, 1973]. In this application the maximum melt factor varied from 3.0 mm/day in the northern part of the Columbia basin to 7.2 mm/day in the southern part. It was kept constant at 3.0 mm/day for the Delaware basin. The minimum melt factor varied from 0.8 mm/day for the northern part of the Columbia basin and all of the Delaware basin to 4.0 mm/day in the southern part of the Columbia basin.

4.3.2. Vegetation Parameters. Land cover classes were assigned to each grid cell on the basis of a global land cover classification with a spatial resolution of 1° latitude and longitude [*DeFries and Townshend*, 1994]. This classification is based on satellite derived normalized difference vegetation index (NDVI) values and is specifically developed to aid in global change research. Values for the vegetation parameters in each of the classes are given in Table 1, and are adapted from *Sellers et al.* [1994]. Average monthly LAI values were based on a 2-year time series of satellite-derived NDVI values [*Sellers et al.*, 1994, 1996]. Roughness lengths, z_0, and displacement heights, d_0, were calculated on the basis of assumed average vegetation heights, h, following *Calder* [1993]. Values for the architectural resistance were those reported by *Ducoudré et al.* [1993]. Each grid cell was assumed to have a total vegetation coverage of 100%, except for land cover class 7, which consists of either moss and lichens or shrubs and bare soil and which was assumed to have a vegetation coverage of only 10% (the remaining 90% was assumed to consist of bare

Table 2. Ranges of Soil Parameters for the Columbia and Delaware River Basins

Soil Parameter	Columbia	Delaware
Infiltration parameter b_i	0.1–0.25	0.25
Total soil moisture $W_{c,tot}$, mm	250–1500	300–400
Fraction of maximum base flow D_s	0.035–0.0475	0.0125
Maximum base flow D_m, mm d^{-1}	5–11	9
Fraction of maximum soil moisture of layer 2 W_s	0.7–0.95	0.25
Ratio of soil moisture in layer 2 to layer 1	1–2	2.3
Pore size distribution index B_p	0.267	0.286
Saturated hydraulic conductivity K_s, mm d^{-1}	25–350	400

soil). Because of the spatial resolution of the land cover classification, only one vegetation class other than bare soil was present in each grid cell, although VIC-2L can handle an arbitrary number of vegetation classes per grid cell.

4.3.3. Soil Parameters. The soil parameters were estimated manually by comparing naturalized monthly streamflow hydrographs with modeled monthly hydrographs at key locations where long-term streamflow data were available. Naturalized monthly streamflow data for the Columbia River were obtained from the *Bonneville Power Administration* [1993] for the period October 1948 to September 1988. These data have been adjusted for reservoir storage effects, reservoir evaporation, and withdrawals. The period October 1948 to September 1960 was used for calibration at nine locations, and the remainder was used for testing. Naturalized streamflow data for the Delaware River were obtained from the *U.S. Army Corps of Engineers* [1981] in the form of modified local inflows (i.e., reservoir storage changes removed) for 67 sites, covering the 60-year period 1927–1987. These local inflows were accumulated to produce calibration time series for three locations in the Delaware basin. The period October 1948 to September 1960 was used for calibration, and the period October 1960 to September 1987 was used for testing.

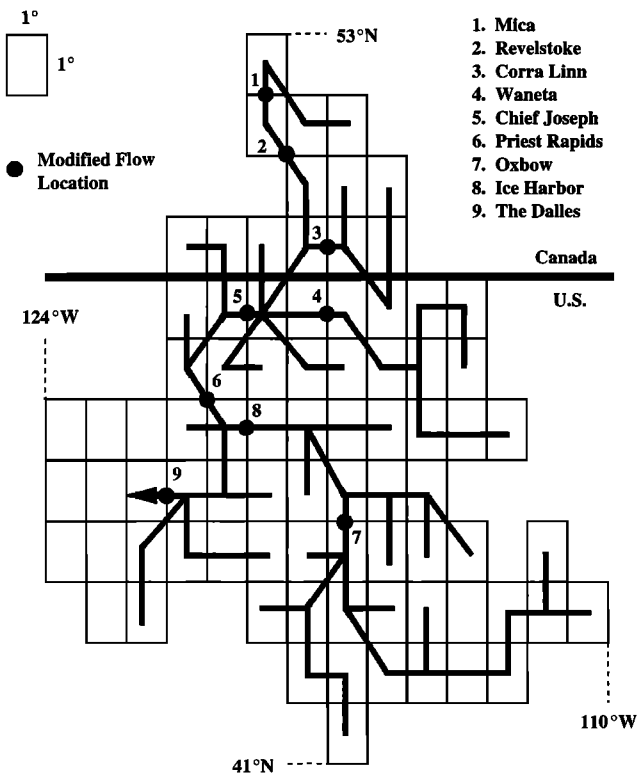

Figure 1. The 1° × 1° schematic river network for the Columbia River basin indicating the basin boundary and locations of the nine calibration points.

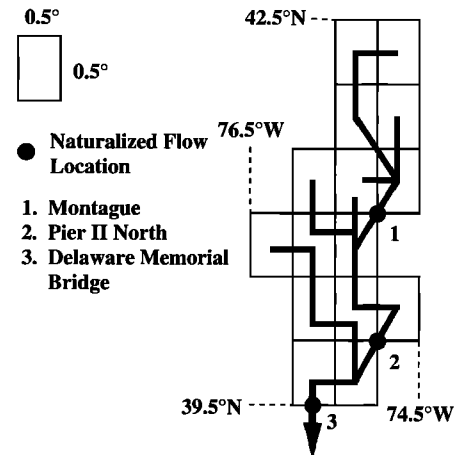

Figure 2. The 0.5° × 0.5° schematic river network for the Delaware River basin indicating the basin boundary and the location of the three calibration points.

The soil parameters with the largest effects on the hydrograph shape at the monthly timescale were the infiltration capacity shape parameter, b_i; the total soil moisture capacity in layer 1 and 2, $W_{c,tot}$; the maximum base flow parameter, D_m; and the fraction of maximum subsurface flow, W_s. W_s represents the fraction of maximum base flow at which the base flow formulation changes from a linear to a nonlinear function of soil moisture. An increase in b_i will generally result in higher peak flows as well as larger annual runoff volumes. The higher peak flows occur because a larger portion of the grid cell is saturated at lower soil moisture contents. Since this water is not stored in the soil, the soil moisture storage remains lower, resulting in lower annual evapotranspiration and higher runoff.

An increase in $W_{c,tot}$ allows more soil moisture storage and thus suppresses runoff peaks while at the same time increasing the base flow recession. The stored soil moisture enables higher base flow and evapotranspiration rates in months with a precipitation deficit. Consequently, an increase in $W_{c,tot}$ leads to lower annual runoff volumes. An increase in the base flow parameters D_m and D_s leads to increased base flow and, consequently, lower annual evaporation and higher runoff. The residual soil moisture, which represents the immobile fraction, was set to zero.

The range of soil moisture parameters used for the Columbia and Delaware basins is given in Table 2. Although it is somewhat counterintuitive, the largest values of $W_{c,tot}$ were used in the northern part of the Columbia basin, which is characterized by high elevations, high precipitation, and low winter temperatures. Each winter a deep snowpack develops in this region, lasting well into the summer at the higher elevations and remaining year-round at the highest peaks. Although mountainous areas are often characterized by shallow soils, the large value of $W_{c,tot}$ (1500 mm in this case) appears to be an artifact of the modeling approach. Only four elevation bands were used in the snow model, which has the result that the

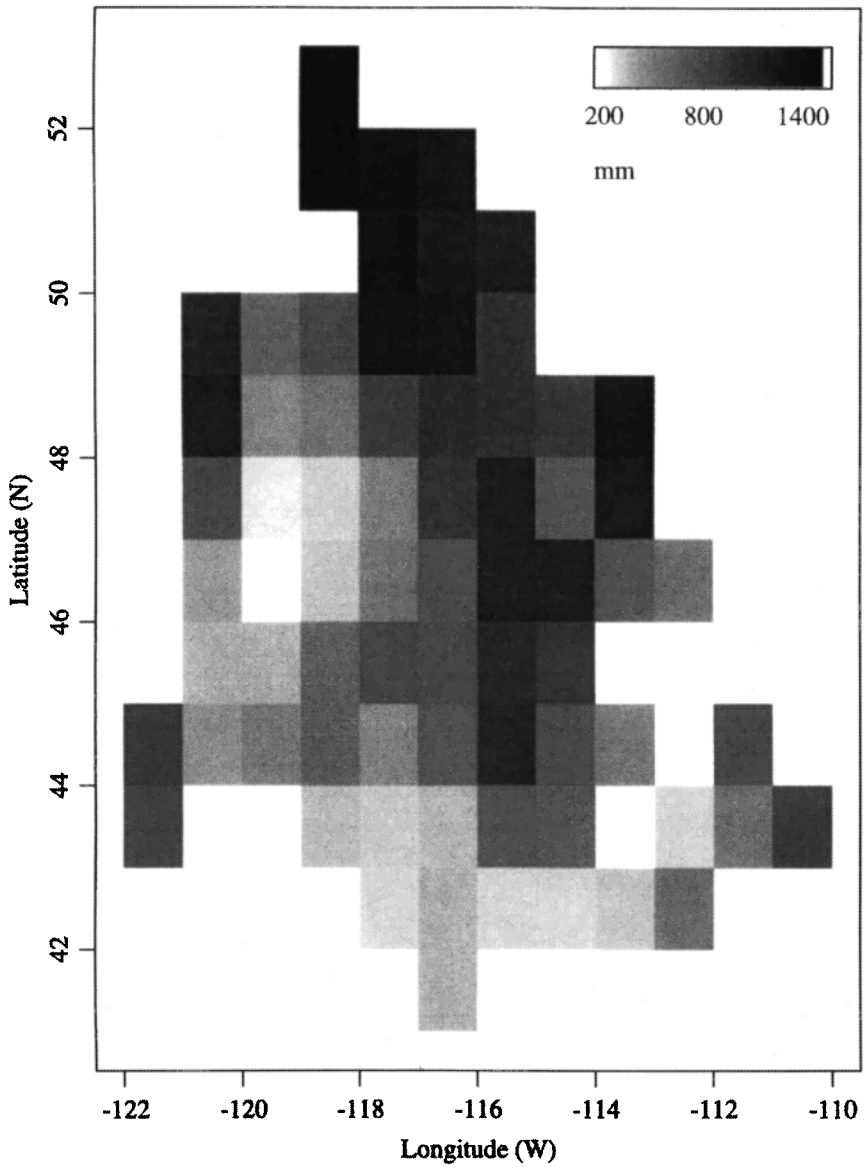

Figure 3. Mean annual precipitation in millimeters for the Columbia River basin.

snowpack at the highest elevations tends to melt too early in the season. The VIC-2L model compensates for this early melting by storing part of this moisture in a thick soil layer, and releasing it as base flow later in the season. The smallest values of $W_{c,\mathrm{tot}}$ (300 mm) were estimated for the northern part of the Delaware basin (except for one grid cell in the Columbia basin, which had a value for $W_{c,\mathrm{tot}}$ of 250 mm), where precipitation is fairly evenly distributed throughout the year and interseasonal soil moisture storage changes play only a minor role.

4.4. River Networks

The schematized river networks for the Columbia and Delaware Rivers, including the basin boundaries and the calibration nodes, are shown in Figures 1 and 2, respectively. The Columbia basin was overlain by 71 1° × 1° grid cells, with The Dalles the farthest downstream point considered. The Delaware basin was overlain by 13 0.5° × 0.5° grid cells, with the Delaware Memorial Bridge as the most downstream location on the river. Flow calibration points were selected on the basis of proximity to the edge of a grid cell and the requirement that they needed to drain significant parts of the basin. From Figure 2 it may appear as if the routing model assumption that all flow from a grid cell must exit in one direction is not met. However, for the Delaware, the routing model was run separately for each of the three major subbasins, and the resulting monthly runoff values were added to provide the total monthly runoff. This approach was justified because the total travel time in the Delaware River is on the order of a few days. Flow velocities in the routing model were adjusted manually, resulting in values from 0.5 to 2.0 m/s for the Columbia and 1.0 m/s for the Delaware. These values do not represent actual channel velocities, since the travel distance between two grid cells is taken as the distance between their centers. The numbers therefore reflect effective flow velocities. They are comparable to the values used for similar purposes by *Miller et al.* [1994].

5. Results

The modeling results for the two test basins, the Columbia and Delaware, are presented in this section. The results gen-

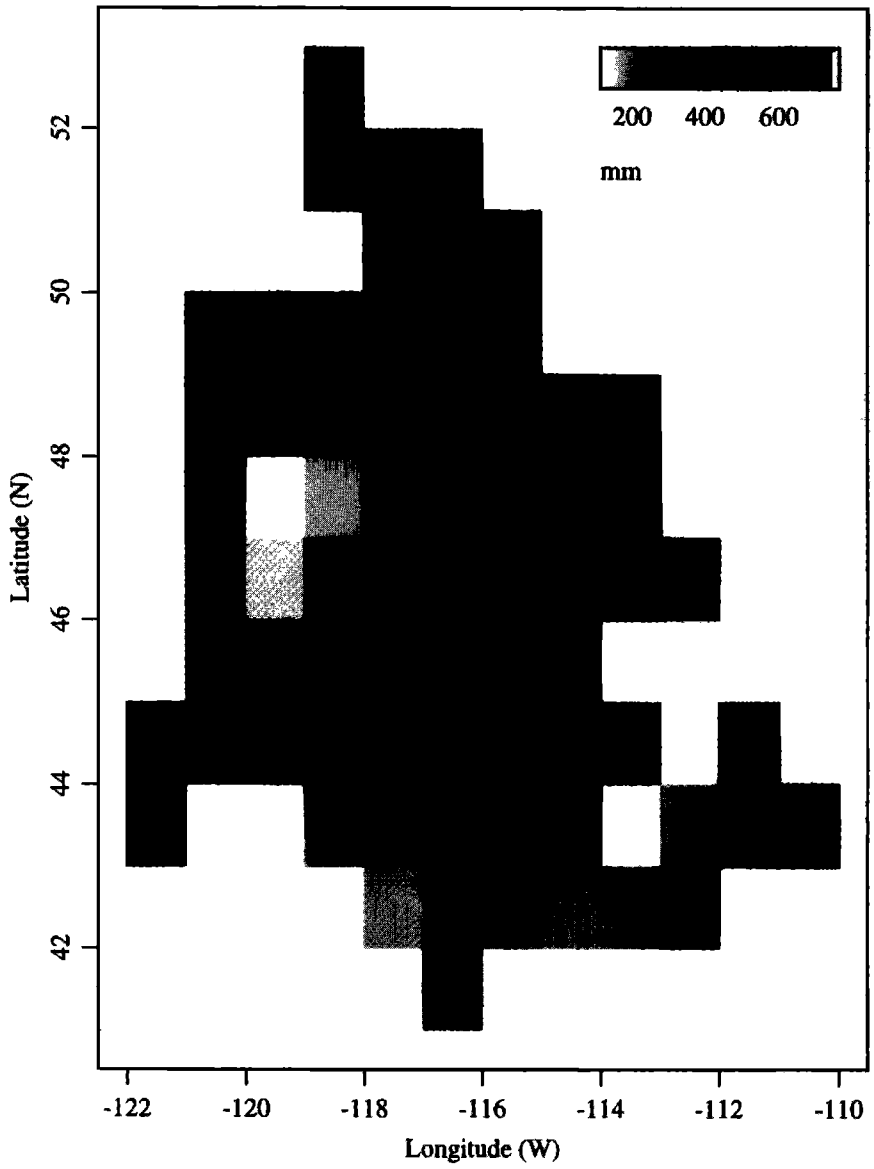

Figure 4. Model-predicted mean annual evapotranspiration in millimeters for the Columbia River basin.

erally take one of two forms: maps of the distribution of hydrologic variables such as mean annual evapotranspiration or monthly time series of such quantities as streamflow at selected locations. To compare simulated and naturalized flows, the relative bias and the relative root mean square error (RRMSE) were calculated annually and for 3-month seasons. The relative bias was calculated as

$$\text{bias} = \frac{\overline{Q_s} - \overline{Q_n}}{\overline{Q_n}} \times 100\%$$

and the RRMSE was calculated as

$$\text{RRMSE} = \frac{\left[(1/n)\sum_{i=1}^{n}(Q_{s,i} - Q_{n,i})^2\right]^{1/2}}{\overline{Q_n}}$$

where Q_s is the simulated flow volume during a period, Q_n is the naturalized flow during the same period, and n is the number of periods.

5.1. Columbia River Basin

Figure 3 shows the spatial distribution of the mean annual precipitation over the Columbia basin, which ranges from 204 to 1508 mm. Precipitation tends to be highest along the northern and western basin boundaries, with the highest amounts in the Canadian part of the basin. Mean annual evapotranspiration predicted by the model for the period October 1948 to September 1988, the entire period for which the model was run, is shown in Figure 4 and ranges from 145 to 732 mm. Although precipitation is highest in the north, the highest evapotranspiration values are found in the eastern part of the basin, where temperatures are higher. Evaporation ratios, defined as the ratio of mean annual evapotranspiration to mean annual precipitation, were as high as 0.887 in the drier parts of the basin and as low as 0.191 in the north. The mean annual runoff varied from 34 to 1219 mm, with the lowest values occurring in the southeastern part of the basin and in the rain shadow of Mount Rainier and highest values occurring in the north. Since the long-term soil moisture change is approxi-

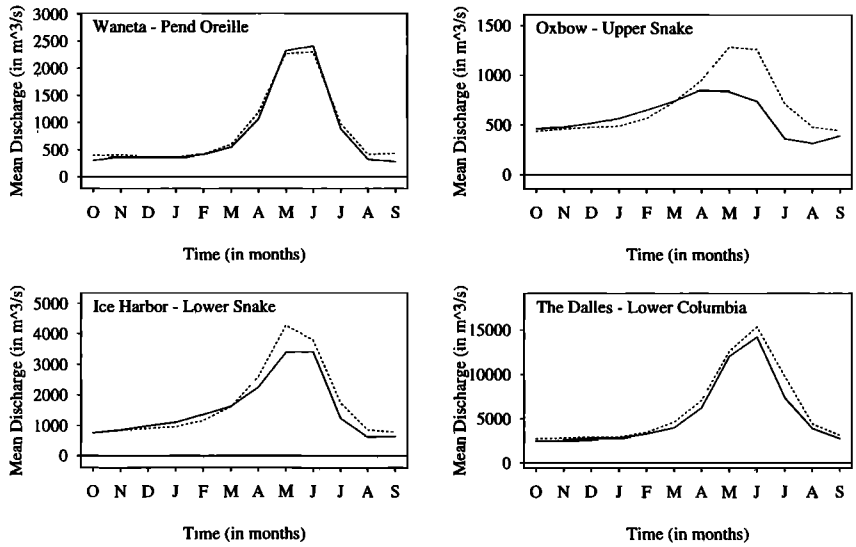

Figure 5. Mean monthly test period hydrographs for four locations in the Columbia River basin. Location names are as in Figure 1. Naturalized flow denoted by solid lines, and simulated flow denoted by dashed lines.

mately zero, the sum of the mean annual runoff and mean annual evapotranspiration was compared with the mean annual precipitation as a check to verify mass conservation.

Figure 5 shows the mean monthly hydrographs for the test period, October 1960 to September 1988, for four locations in the basin. The hydrograph at Waneta near the mouth of the Pend Oreille in the northeastern part of the basin is typical of the northern part of the basin, with a strong snowmelt peak in

Table 3. Comparison Between Modeled and Naturalized Flows for the Nine Calibration Locations in the Columbia River Basin for Annual and Seasonal Biases and Relative Root Mean Square Errors

	Calibration, 1948–1960					Test, 1960–1988				
Statistic	Annual	OND	JFM	AMJ	JAS	Annual	OND	JFM	AMJ	JAS
					Mica					
Bias	9.8	28.4	46.8	7.6	5.2	10.1	36.9	30.6	0.2	11.0
RRMSE	0.176	0.440	0.525	0.147	0.286	0.142	0.455	0.331	0.107	0.239
					Revelstoke					
Bias	2.1	8.2	23.0	1.5	−0.7	0.1	15.7	15.2	−5.1	−0.2
RRMSE	0.130	0.315	0.324	0.100	0.253	0.087	0.292	0.210	0.103	0.188
					Corra Linn					
Bias	0.0	7.9	27.7	−2.0	−6.2	8.8	13.2	20.0	6.8	8.1
RRMSE	0.116	0.306	0.332	0.119	0.188	0.155	0.259	0.279	0.156	0.261
					Waneta					
Bias	0.8	3.6	9.7	−3.6	8.8	5.6	13.4	5.6	−0.5	23.6
RRMSE	0.114	0.148	0.147	0.148	0.232	0.140	0.212	0.198	0.156	0.357
					Chief Joseph					
Bias	0.8	9.4	20.8	−3.7	−0.3	6.0	18.6	12.5	1.2	8.0
RRMSE	0.085	0.191	0.223	0.114	0.125	0.107	0.236	0.172	0.112	0.166
					Priest Rapids					
Bias	4.0	7.1	20.2	1.3	2.3	9.6	18.4	12.1	5.6	12.9
RRMSE	0.095	0.185	0.219	0.120	0.120	0.133	0.237	0.172	0.126	0.197
					Oxbow					
Bias	2.4	−9.1	−11.1	9.6	21.5	20.2	−5.9	−8.4	43.9	54.0
RRMSE	0.071	0.133	0.178	0.157	0.256	0.230	0.143	0.213	0.509	0.584
					Ice Harbor					
Bias	1.1	−7.2	−7.2	4.1	9.1	11.2	−3.9	−8.5	17.9	34.2
RRMSE	0.085	0.118	0.123	0.135	0.165	0.157	0.120	0.175	0.262	0.377
					The Dalles					
Bias	4.3	0.8	10.4	2.0	7.6	11.8	10.2	9.3	7.8	23.6
RRMSE	0.093	0.122	0.145	0.117	0.131	0.150	0.149	0.168	0.149	0.273

See Figure 1 for locations. OND, October–December; JFM, January–March; AMJ, April–June; JAS, July–September.

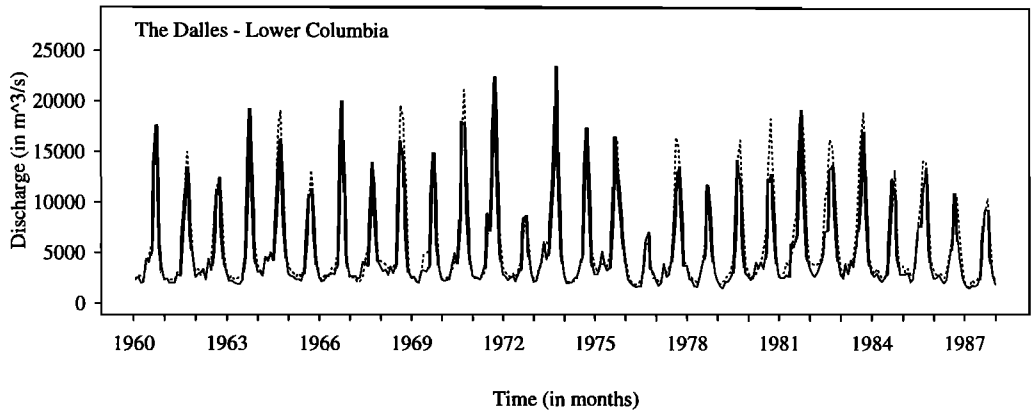

Figure 6. Time series of naturalized (solid lines) and simulated (dashed lines) monthly discharge at The Dalles, Columbia River, for the test period.

late spring–early summer, when flows are on average about five times higher than those during the fall and winter months. Modeled flows for this part of the basin closely match the naturalized flows, both in timing and in magnitude. Table 3 shows the relative bias of the mean annual and seasonal runoff volumes for the modeled and naturalized flows as well as the RRMSE for both the calibration period and the test period.

The hydrograph at Oxbow Dam on the Upper Snake River in the southeastern part of the basin shows the poorest fit both in timing and in magnitude, of any of the nine locations. The overprediction of the spring peak and annual runoff amount is even more pronounced during the test period. Although the area upstream of this station accounts for about a quarter of the total basin area, the amount of runoff produced here forms only one tenth of the total basin runoff. At Ice Harbor, on the Lower Snake River, observed and simulated flow are again in good agreement, both for the calibration and test period, which indicates that the runoff from the area between Oxbow and Ice Harbor must be underpredicted. The discrepancy between modeled and naturalized flows at Oxbow Dam may be the result of a number of factors. This area is the driest part of the basin, and most hydrological models perform poorer in dry regions. *Abdulla and Lettenmaier* [1997] in their application of the VIC-2L model to the Arkansas-Red basin also noted that the model performance was the worst in arid and semiarid regions, in part because the VIC-2L model does not have an explicit mechanism to produce infiltration excess flow. Perhaps more importantly in the Snake River basin, groundwater dominates the runoff response of much of the upper basin, as suggested by the fact that the streamflow has a much more damped seasonal cycle than does the precipitation. VIC-2L does not include a mechanism to account for deep groundwater recharge and drainage to streams. Finally, the routing model requires that each grid cell flow in only direction, and thus each cell has to be assigned to one subbasin or another. This can result in relatively large errors for dry subbasins such as the Snake. In addition, the routing model assumes that each of the calibration locations lies at the edge of a grid cell, which in reality will often not be the case. For a site such as Ice Harbor, which collects runoff from a large area, these edge effects are relatively unimportant.

Spring runoff at the northern-most locations (Mica Dam and Revelstoke Dam) was overpredicted as well, mainly because the snow model does not allow for sublimation, and because four elevation bands may not always capture the snow pack dynamics in enough detail.

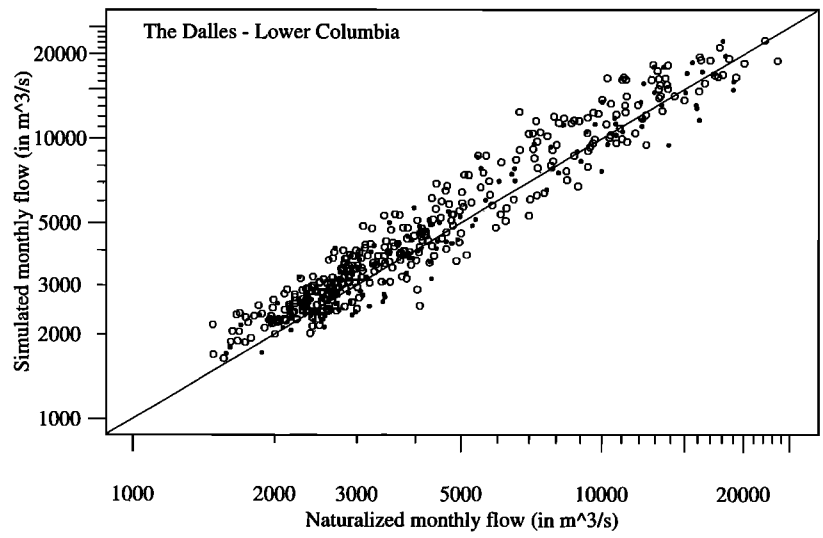

Figure 7. Scatter plot of simulated and naturalized monthly discharge during the calibration period (solid circles) and the test period (open circles) at The Dalles, Columbia River.

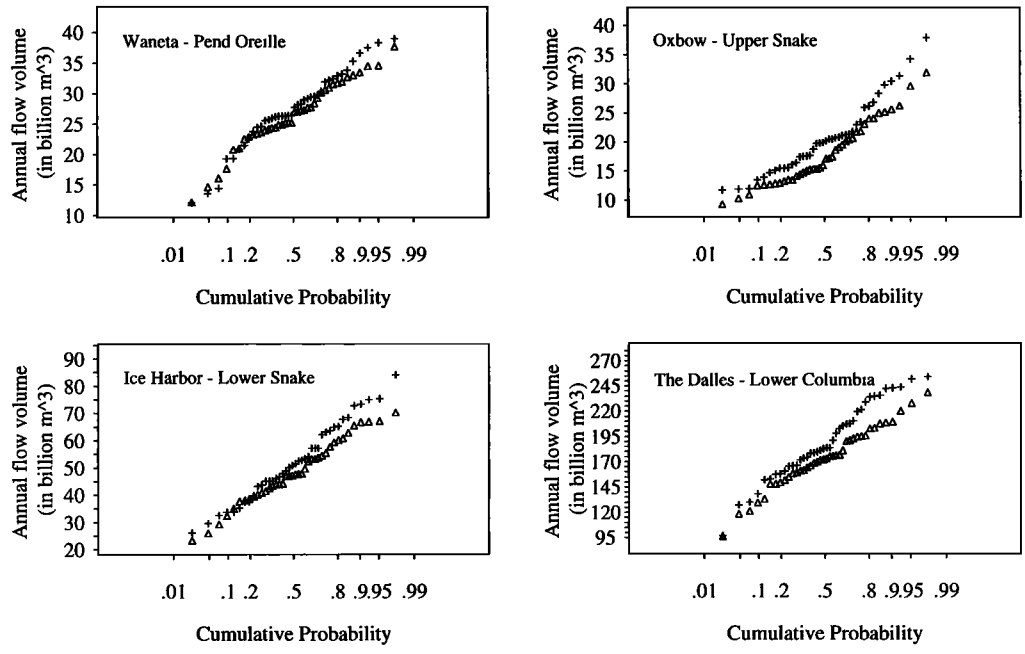

Figure 8. Cumulative probability distribution of naturalized (triangles) and simulated (pluses) annual flow volumes for four locations in the Columbia River basin.

Figure 6 shows that the time series of monthly simulated and naturalized flows for the Columbia River at The Dalles (the most downstream point on the Columbia River considered) is well simulated during the test period, although the discharge is on average slightly overpredicted during all seasons. Figure 7 shows the same results as a scatter plot for both the calibration and test period. The simulated flows have the strongest relative bias during low-flow months, particularly during the test pe-

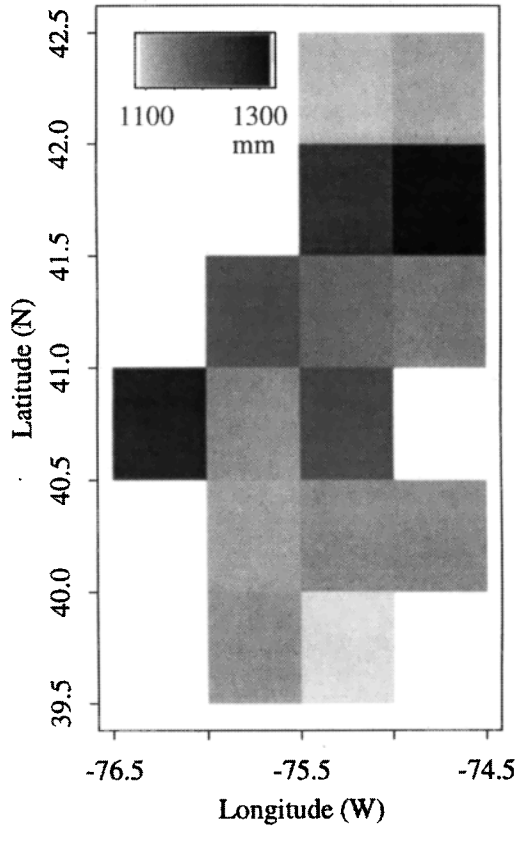

Figure 9. Mean annual precipitation in millimeters for the Delaware River basin.

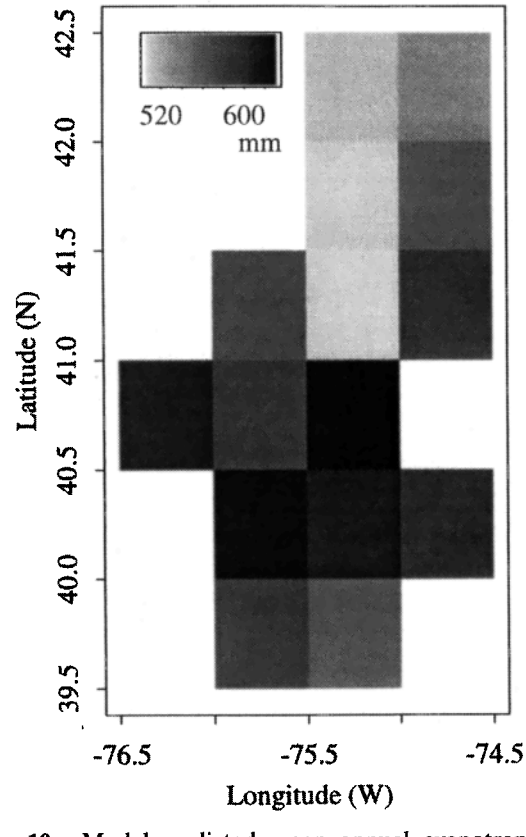

Figure 10. Model-predicted mean annual evapotranspiration in millimeters for the Delaware River basin.

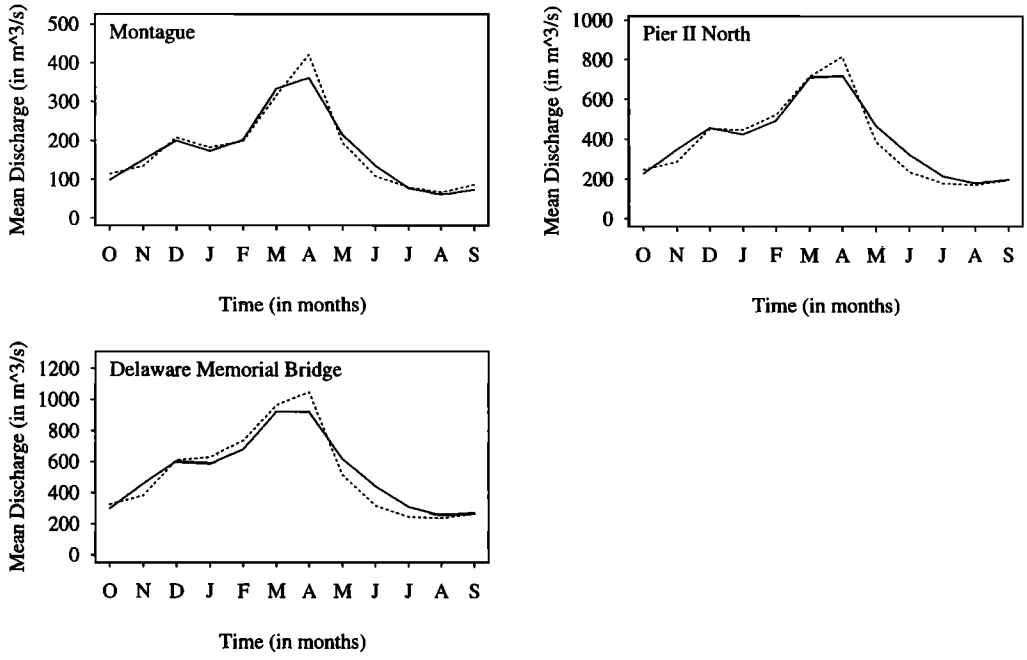

Figure 11. Mean monthly test period hydrographs for three locations in the Delaware River basin. Location names are as in Figure 2. Naturalized flow denoted by solid lines, and simulated flow denoted by dashed lines.

riod. The lowest flows in the Columbia River basin occur from midsummer to early fall, and the seasonal bias in flow volume for the period July–September is 23.6% for the test period (Table 3). For the other seasons this bias ranges from 7.8% to 10.2%. During the calibration period the mean annual simulated flow volume is 4.3% larger than the mean annual naturalized flow volume, while during the test period the simulated flow volume is 11.8% larger than the naturalized flow volume.

The variability in annual flow volumes is also well reproduced by the VIC-2L model, as shown in Figure 8. For Waneta, Ice Harbor, and The Dalles the model produces the full range of observed flow volumes, although the model simulates peak flows at the Dalles somewhat larger than those observed. For Oxbow, the model consistently overpredicts the annual flows, for the reasons discussed above.

5.2. Delaware River Basin

The distribution of mean precipitation over the Delaware basin is much more homogeneous (Figure 9) than that over the Columbia basin. This is mainly a result of scale (the area of the Delaware basin is only one twentieth the area of the Columbia basin) and smaller topographic variations. Since temperature also varies only moderately over the basin, the mean annual evaporation demonstrates the same uniformity, varying from a low of 507 mm to a high of 630 mm (Figure 10). Similarly, the range in the evaporation ratio (0.406 to 0.556) is much smaller than that in the Columbia basin.

The hydrographs for the calibration and test periods (Figure 11) demonstrate that the runoff is more evenly distributed throughout the year, with higher runoff during winter and spring, and a small snowmelt peak in April for the northern part of the basin. During both the calibration and testing periods, and for all locations, the flow is slightly overpredicted during fall and spring and underpredicted during midsummer. The total annual flow volume is underpredicted by 1.4% during the test period (Table 4). As discussed in section 4.3.3, the soil moisture capacities used to model the northern part of the

Table 4. Comparison Between Monthly Modeled and Naturalized Flows for the Three Calibration Locations in the Delaware River Basin for Annual and Seasonal Biases and Relative Root Mean Square Errors

	Calibration, 1948–1960					Test, 1960–1987				
Statistic	Annual	OND	JFM	AMJ	JAS	Annual	OND	JFM	AMJ	JAS
					Montague					
Bias	1.0	−11.5	−0.7	4.2	26.9	1.3	1.5	−1.7	1.6	10.0
RRMSE	0.064	0.158	0.163	0.182	0.384	0.098	0.230	0.157	0.234	0.284
					Pier II North					
Bias	1.2	−11.6	7.1	−0.4	13.7	−2.3	−4.3	3.4	−4.8	−7.9
RRMSE	0.056	0.167	0.134	0.117	0.247	0.112	0.223	0.134	0.225	0.239
					Delaware Memorial Bridge					
Bias	1.1	−11.4	9.1	−2.2	10.1	−1.4	−3.2	6.4	−5.1	−10.4
RRMSE	0.060	0.170	0.143	0.117	0.200	0.113	0.217	0.142	0.211	0.253

See Figure 2 for locations. OND, October–December; JFM, January–March; AMJ, April–June; JAS, July–September.

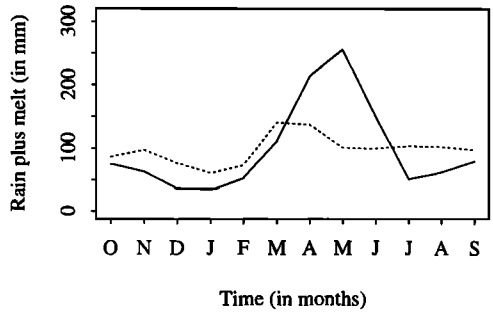

Figure 12. Mean monthly rain-plus-melt series for the northern part of the Delaware River basin (dashed lines) compared with the rain-plus-melt series for four cells in the Columbia River basin (solid lines).

Delaware basin are much lower than those used for the Columbia River, and it was argued that this was a result of the more homogeneous distribution of rain plus melt throughout the year. Figure 12 shows the mean monthly rain plus melt series for the northern part of the Delaware basin, and compares it with the mean monthly series for four cells in the middle part of the Columbia basin that have similar annual average precipitation. For the Columbia basin cells the mean $W_{c,\mathrm{tot}}$ was 1210 mm, while for the Delaware basin, $W_{c,\mathrm{tot}}$ was only 300 mm.

6. Conclusions

A grid-based land surface scheme to accurately predict monthly hydrographs for continental-scale river basins has been described. The method was implemented at a 1° grid scale for the Columbia basin and at a 0.5° grid scale for the Delaware basin. Both annual runoff volumes as well as hydrograph shape were simulated with an acceptable degree of accuracy, with mean annual runoff volumes during the test periods predicted to within 11.8% for the Columbia, and 1.4% for the Delaware. Although the approach performed well for most of the basin area, it failed in the arid region of the Snake River Plain, apparently owing to the absence of an infiltration excess mechanism in the model and, more importantly, to the strong groundwater-surface water interactions that exist in the upper Snake basin and are not represented in the model. *Abdulla and Lettenmaier* [1997] encountered similar problems with the application of the VIC-2L model in the semiarid and arid regions of the Red-Arkansas basin.

Several refinements of the grid-based VIC-2L model are currently being pursued. One of these is extending the routing scheme to allow flow from one grid cell to exit in more than one direction. This will permit the modeled subbasin areas to be brought into closer agreement with the true basin geography. Another is including an explicit mechanism to allow for systematic differences in subgrid precipitation in grid cells with large orographic effects. Overall, though, the results demonstrate the feasibility of the method for simulating hydrologic fluxes, including streamflow, for large continental-scale catchments.

Acknowledgments. The research on which this paper is based was supported in part by the Electric Power Research Institute under project RP 2938-03, by the National Oceanic and Atmospheric Administration under grants NA56GP0198 and NA566P0249, and by the National Science Foundation under grant EAR-9318898.

References

Abdulla, F. A., and D. P. Lettenmaier, Application of regional parameter estimation schemes to simulate the water balance of a large continental river, *J. Hydrol.*, in press, 1997.

Anderson, E. A., National Weather Service river forecast system—Snow accumulation and ablation model, *NOAA Tech. Memo. NWS HYDRO-17*, 1973.

Ayers, M. A., D. M. Wollock, G. J. McCabe, L. E. Hay, and G. D. Tasker, Sensitivity of water resources in the Delaware River Basin to climate variability and change, *U.S. Geol. Surv. Water Supply Pap. 2422*, 1994.

Bonneville Power Administration, 1990 level modified streamflow 1928–1989, diversion and return flow patterns, summation of depletion adjustments, evaporation adjustments, Columbia river and coastal basins, Portland, Oreg., April 1993.

Blondin, C., Parameterization of land-surface processes in numerical weather prediction, in *Land Surface Evaporation: Measurements and Parameterization*, edited by T. J. Schmugge and J. C. André, pp. 31–54, Springer-Verlag, New York, 1991.

Bras, R. L., *Hydrology: An Introduction to Hydrologic Science*, Addisson-Wesley, Reading, Mass., 1990.

Bristow, K. L., and G. S. Campbell, On the relationship between incoming solar radiation and daily maximum and minimum temperature, *Agric. For. Meteorol.*, *31*, 159–166, 1984.

Brutsaert, W., *Evaporation Into the Atmosphere*, 299 pp., Kluwer Acad., Norwell, Mass., 1982.

Burnash, R. J. C., R. L. Ferral, and R. A. McGuire, A generalized streamflow simulation system: Conceptual modeling for digital computers, U.S. Natl. Weather Serv., Sacramento, Calif., 1973.

Calder, I. R., Hydrologic effects of land-use change, in *Handbook of Hydrology*, chap. 13, edited by D. R. Maidment, McGraw-Hill, New York, 1993.

Daly, C., R. P. Neilson, and D. L. Phillips, A statistical-topographic model for mapping climatological precipitation over mountainous terrain, *J. Appl. Meteorol.*, *33*, 140–158, 1994.

DeFries, R. S., and J. R. G. Townshend, NDVI-derived land cover classifications at a global scale, *Int. J. Remote Sens.*, *15*(17), 3567–3586, 1994.

Dickinson, R. E., A. Henderson-Sellers, P. J. Kennedy, and M. F. Wilson, Biosphere-atmosphere transfer scheme (BATS) for the NCAR community climate model, *NCAR Tech. Note TN-275+STR*, 1986.

Ducoudré, N. I., K. Laval, and A. Perrier, SECHIBA, a new set of parameterizations of the hydrologic exchanges at the land-atmosphere interface within the LMD atmospheric general circulation model, *J. Clim.*, *6*, 248–273, 1993.

Dümenil, L., and E. Todeni, A rainfall-runoff scheme for use in the Hamburg climate model, in *Advances in Theoretical Hydrology: A Tribute to James Dooge, Eur. Geophys. Soc. Ser. on Hydrol. Sci.*, vol. 1, edited by J. P. O'Kane, pp. 129–157, Elsevier, New York, 1992.

Earthinfo Inc., *NCDC Summary of the Day*, vol. 3, Earthinfo Inc., Boulder, Colo., 1991.

Francini, M., and M. Pacciani, Comparative analysis of several conceptual rainfall-runoff models, *J. Hydrol.*, *122*, 161–219, 1991.

Gray, D. M., and T. D. Prowse, Snow and floating ice, in *Handbook of Hydrology*, chap. 7, edited by D. R. Maidment, McGraw-Hill, New York, 1993.

Henderson-Sellers, A., A. J. Pitman, P. K. Love, P. Irannejad, and T. H. Chen, The Project for Intercomparison of Land Surface Schemes (PILPS): Phases 2 and 3, *Bull. Am. Meteorol. Soc.*, *94*, 489–503, 1995.

Kalnay, E., et al., The NCEP/NCAR 40-year reanalysis project, *Bull. Am. Meteorol. Soc.*, *77*(3), 437–471, 1996.

Kimball, J., S. W. Running, and R. R. Nemani, An improved method for estimating surface humidity from daily minimum temperature, *Agric. For. Meteorol.*, in press, 1997.

Koster, R. D., and M. J. Suarez, Modeling the land surface boundary in climate models as a composite of independent vegetation stands, *J. Geophys. Res.*, *97*, 2697–2715, 1992.

Kouwen, N., E. D. Soulis, A. Pietroniro, J. Donald, and R. A. Harrington, Grouped response units for distributed hydrologic modeling, *J. Water Resour. Plann. Manage.*, *119*(3), 289–305, 1993.

Kuhl, S. C., and J. R. Miller, Seasonal river runoff calculated from a global atmospheric model, *Water Resour. Res.*, *28*, 2029–2039, 1992.

Liang, X., D. P. Lettenmaier, E. F. Wood, and S. J. Burges, A simple hydrologically based model of land surface water and energy fluxes

for general circulation models, *J. Geophys. Res.*, *99*(D7), 14,415–14,428, 1994.

Liston, G. E., Y. C. Sud, and E. F. Wood, Evaluating GCM land surface hydrology parameterizations by computing river discharges using a runoff routing model: Application to the Mississippi basin, *J. Appl. Meteorol.*, *33*, 394–405, 1994.

Miller, J. R., and G. L. Russell, The impact of global warming on river runoff, *J. Geophys. Res.*, *97*(D3), 2757–2764, 1992.

Miller, J. R., G. L. Russell, and G. Caliri, Continental-scale river flow in climate models, *J. Clim.*, *7*, 914–928, 1994.

Riverside Technologies, Inc, Users guide to the Columbia River Forecast system, report prepared for Bonneville Power Admin. in conjunction with Harza Engineering, Dec. 1994.

Rowntree, P. R., and J. Lean, Validation of hydrological schemes for climate models against catchment data, *J. Hydrol.*, *155*, 301–323, 1994.

Russel, G. L., and J. R. Miller, Global river runoff calculated from a global atmosphere general circulation model, *J. Hydrol.*, *116*, 241–254, 1990.

Sausen, R., S. Schubert, and L. Dümenil, A model of river runoff for use in coupled atmosphere-ocean model, *J. Hydrol.*, *155*, 337–352, 1994.

Sellers, P. J., Y. Mintz, Y. C. Sud, and A. Dalcher, A simple biosphere model (SiB) for use within general circulation models, *J. Atmos. Sci.*, *43*, 505–531, 1986.

Sellers, P. J., S. O. Los, C. J. Tucker, C. O. Justice, D. A. Dazlich, G. J. Collatz, and D. A. Randall, A global 1 by 1 degree NDVI data set for climate studies, 2, The generation of global fields of terrestrial biophysical parameters from the NDVI, *Int. J. Remote Sens.*, *15*(17), 3519–3545, 1994.

Sellers, P. J., S. O. Los, C. J. Tucker, C. O. Justice, D. A. Dazlich, G. J. Collatz, and D. A. Randall, A revised land surface parameterization (SiB2) for atmospheric GCMs, II, The generation of global fields of terrestrial biophysical parameters from satellite data, *J. Clim.*, *9*, 706–737, 1996.

Shuttleworth, W. J., Evaporation, in *Handbook of Hydrology*, chap. 4, edited by D. R. Maidment, McGraw-Hill, New York, 1993.

Stamm, J. F., E. F. Wood, and D. P. Lettenmaier, Sensitivity of a GCM simulation of global climate to the representation of land surface hydrology, *J. Clim.*, *7*, 1218–1239, 1994.

U.S. Army Corps of Engineers, Daily flow model of the Delaware River Basin, main report, Camp Dressler and McKee, Annandale, Va., 1981.

U.S. Geological Survey, River basins of the United States: The Columbia, U.S. Geological Survey, U.S. Govt. Print. Off., Washington, D. C., 1994.

Wallis, J. R., D. P. Lettenmaier, and E. F. Wood, A daily hydroclimatological data set for the continental U.S., *Water Resour. Res.*, *27*, 1657–1664, 1991.

Wetzel, S. W., A hydrologic model for predicting the effects of climate change, B.Sc. thesis, Dep. of Civ. Eng. and Oper. Res., Princeton Univ., Princeton, N. J., 1994.

Wigmosta, M., L. Vail, and D. P. Lettenmaier, A distributed hydrology-vegetation model for complex terrain, *Water Resour. Res.*, *30*, 1665–1679, 1994.

Wood, E. F., Global scale hydrology: Advances in land surface modeling, *U.S. Natl. Rep. Int. Union Geol. Geophys. 1987–1990*, *Rev. Geophys.*, *29*, 193–201, 1991.

World Meteorological Organization (WMO), Arctic Climate System Study (ACSYS), Initial implementation plan, *WCRP-85*, *WMO/TD*, no. 627, Geneva, 1994.

Zhao, R. J., Y. L. Zhang, L. R. Fang, X. R. Liu, and Q. S. Zhang, The Xinanjiang model, in *Hydrological Forecasting*, *Proceedings Oxford Symposium*, *IAHS Publ. 129*, pp. 351–356, 1980.

D. P. Lettenmaier and B. Nijssen, Department of Civil Engineering, University of Washington, Box 352700, Seattle, WA 98195. (e-mail: dennisl@u.washington.edu; nijssen@u.washington.edu)

X. Liang and E. F. Wood, Department of Civil Engineering and Operations Research, Princeton University, Princeton, NJ 08544.

S. W. Wetzel, Applied Ocean and Engineering Department, Woods Hole Oceanographic Institution, Woods Hole, MA 02543.

(Received November 5, 1995; revised November 11, 1996; accepted November 11, 1996.)